ACADEMIA ROMÂNĂ

Revue Roumaine de Chimie

https://www.icf.ro/rrch/

Rev. Roum. Chim.,
2026, *71*(3–4), 205–215
DOI: 10.33224/rrch.2026.71.3-4.05

SYNTHESIS AND ANTIBACTERIAL ACTIVITY OF Sr-DOPED Co_3O_4 NANOPARTICLES

Ouardia SEBBAH,[a] Lamia BENNABI,[b,c] Hadj BENHEBAL,[d] F.Zohra CHOULAK,[d] Samir KADI,[e] Abdelhalim ZOUKEL,[f] Faiza BENNABI[g] and Stéphanie D. LAMBERT[h]

[a] Synthesis and Catalysis Laboratory, Ibn Khaldoun University, Tiaret, Algeria
[b] Faculty of science and technology, department of Science of Matter, University of Belhadj Bouchaib Ain Temouchent, Algeria
[c] Laboratory of LCOPM, University of Djillali Liabes Sidi Bel A bes, Algeria
[d] Department of chemistry, Ibn Khaldoun University Tiaret, Algeria
[e] Laboratory of Plant Physiology Applied to Above Ground Culture, Department of Nature and Life Sciences, University of Tiaret, BP 78 Zaaroura, Tiaret 14000, Algeria
[f] Laboratory Physico-Chemistry of Materials, Laghouat University, Laghouat, Algeria
[g] Department of Environmental Sciences, Faculty of Natural and Life Sciences, University of Djillali liabes, Sidi Bel Abbes 22000, Algeria
[h] Department of Chemical Engineering–Nanomaterials, Catalysis and Electrochemistry, B6a, University of Liege, 4000 Liege, Belgium

Received July 19, 2025

Undoped and Sr-doped spinel structured Co_3O_4 were successfully prepared by sol-gel process for antibacterial application. The formation of Sr-doped Co_3O_4 nanoparticles with good crystalline nature of the samples was identified by X-ray powder diffraction analysis. The crystallite size (D) and other related structural properties are calculated. Antibacterial activity against Gram-positive and Gram-negative bacteria has been tested. The calculated crystallites size of the Co_3O_4:SrNPs were increased from 36,58 nm to 37,47 nm on increased the concentration of strontium. Fourier-transform infrared spectroscopy showed the stretching vibration of (Sr^{2+}–O^{2-}) and (Co^{3+}–O^{2-}) with respective bands at 578 and 667 cm^{-1}. The uniform distribution of agglomerated spherical particles was observed by scanning electron microscopy. The Sr-doped Co_3O_4 nanoparticles demonstrated enhanced antimicrobial efficacy, with inhibition zones up to 29 mm (C. albicans) and MIC values between 3.12–6.25 mg/L. Statistical analysis ($p < 0.05$) confirmed that increasing Sr content significantly improved the antimicrobial performance, consistent with surface charge reduction (from −16.2 mV to −6.69 mV) and enhanced ROS generation. The values inhibition zone diameters obtained of Sr-doped Co_3O_4 are comparable to the standard positive and negative control.

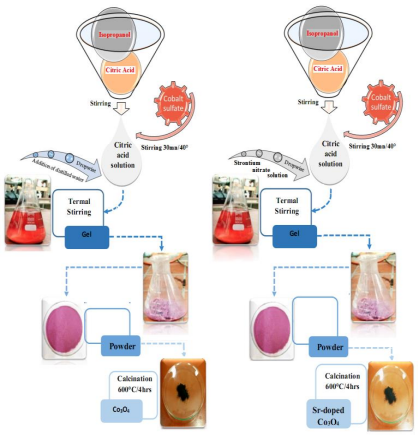

INTRODUCTION

Clean drinking water, free from contaminants, is an essential resource for the life of all living beings.[1] With the increase in pollution levels, many diseases are caused by bacterial pathogens, thus posing significant health challenges in many parts of the world.[2] Due to the properties of nanomaterials, nanotechnology offers a great opportunity for therapeutic application against antibacterial infections.[3] Transition metal oxides with mixed oxidation states constitute an important

* Corresponding author: benhebalh@yahoo.fr; benhebal@univ-tiaret.dz

class of nanomaterials.[4] The use of these materials as antimicrobial and antifungal agents offers several advantages: good efficacy even in small quantities against resistant strains of microbial pathogens and good heat resistance. Furthermore, they are non-toxic and are a source of essential minerals for human cells.[5–7] Out of these, spinel tricobalt tetroxide (Co_3O_4) has recently attracted considerable interest and attention in research and for a wide range of technological applications in the field of energy storage devices, environmental remediation and biomedical applications.[8] However, some applications of Co_3O_4 require adjustments to its physicochemical properties because spinel structure tolerates a high concentration of defects.[9] Indeed, doping with metallic elements with multivalent states is an effective approach for tuning the physicochemical properties of these compounds.[10] Due to the absence of d-shell in their electronic structure, alkaline earth metals like strontium (Sr) can be a suitable choice as dopants.[11] Several studies have been reported in the literature on the changes associated with the doping of metal oxides with strontium, notably the improvement of antibacterial activity such as ZnO, CuO, ZrO_2, Cr_2O_3, Ag_2O, TiO_2, SnO_2, CeO_2, MnO_2, Fe_3O_4, $YMnO_3$, $LaMnO_3$, $NdMnO_3$, $CoAl_2O_4$, $MgMn_2O_4$ and Co_3O_4.[12–27] Numerous methods are used for the preparation of metal oxide nanoparticles.[28,29] Most of these synthesis methods require the implementation of difficult experimental conditions, whereas the sol-gel method is a relatively simple, inexpensive and efficient route for the synthesis of high-purity nanoparticles with a controlled size.[30] To the authors' knowledge, the application of strontium-doped cobalt oxide in antibacterial activity has not been explored. Therefore, in this contribution, we present the evaluation of the antibacterial and antifungal activity of Co_3O_4 through Sr tetrahedral doping (3% and 5% wt.) prepared by sol-gel process.

MATERIALS AND METHODS

Chemicals

All chemical products used in this work were of analytical grade without the purification, Cobalt sulfate ($CoSO_4$), Strontium nitrates $Sr(NO_3)_2$, Citric acid ($C_6H_8O_7$), isopropanol (C_3H_6O), Sodium hydroxide (NaOH), Hydrochloric acid (HCl).

Materials synthesis

Pure and strontium-doped Co_3O_4 nanoparticles were prepared by the sol-gel method.

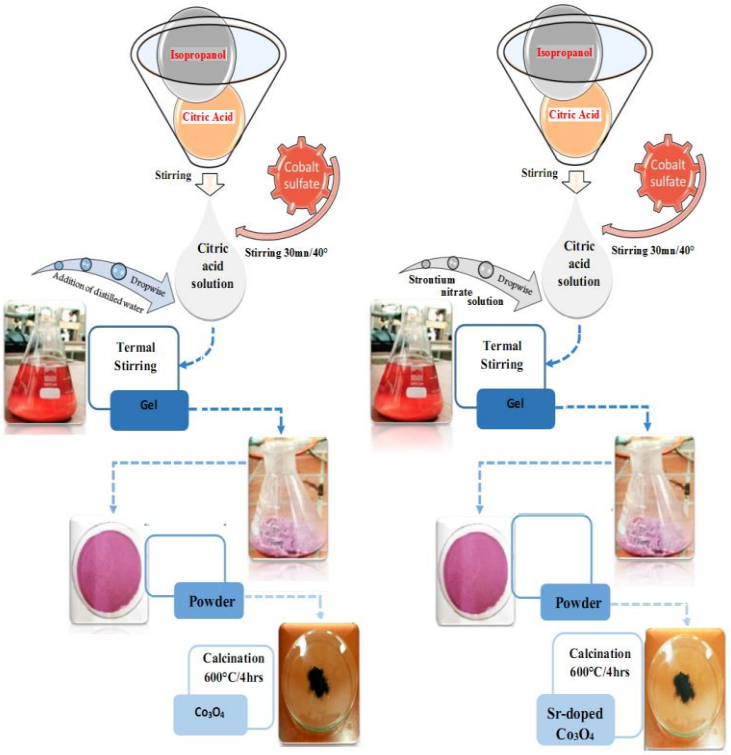

Fig. 1 – Flow chart of pure and Sr-doped cobalt oxide synthesis by sol-gel method.

Cobalt sulfate and strontium nitrate (Sigma Aldrich, research grade, 99% purity) were used as precursors for the synthesis. 4,5 mmol of citric acid was dissolved in 225 mL of isopropanol) and stirred for 30 min at 40 °C, then 1,0 mmol of Cobalt (II) sulphate was added to the previous solution and mixed for 30 min at 40 °C. Another solution prepared by dissolving 0.5 mmol of strontium nitrate in 25 ml of isopropanol was added dropwise to the above mixture and kept under thermal stirring until a viscous gel was formed which dried in a vacuum-drying at 120 °C. The obtaining crust was then carefully ground to obtain a fine powder which was calcined in an electric furnace for 4 h at 600 °C. Finally, the obtained powders were designated as SC, SC3 and SC6, respectively. The experimental procedure for synthesis steps of the undoped and Sr-doped Co_3O_4 nanoparticles was shown in Fig. 1.

Materials characterization

XRD measurements were carried out on a Bruker D8 Twin-Twin powder diffractometer with (CuKα) radiation using a copper anticathode (λ = 1.5406 Å). FTIR spectra of pure and Sr-doped Co_3O_4 were studied using a Shimadzu 8400 Spectrometer in the wave number range from 400 cm^{-1} to 4000 cm^{-1}. The morphology and elemental analysis were investigated with SEM-EDX using Quanta 250 (with tungsten filament from FEI Company). Surface charge was studied by Zeta potential analysis using Zeta-sizer (Malvern Instruments) model.

Antibacterial activity tests

The antibacterial and antifungal activities of the nanoparticle-based formulations (SC, SC3, and SC6) were evaluated against both Gram-negative and Gram-positive microorganisms: *Escherichia coli* (ATCC 25922), *Pseudomonas aeruginosa* (ATCC 27853), *Staphylococcus aureus* (ATCC 25923), and the yeast *Candida albicans* (ATCC 10231).

Agar Diffusion Method

The antimicrobial screening was performed using the agar well diffusion method. Sterile Petri dishes were filled with approximately 15 mL of Mueller–Hinton agar (MHA) for bacteria and for *C. albicans*. Each medium was inoculated with 10 µL of a standardized microbial suspension adjusted to the 0.5 McFarland standards (≈10^6 CFU/mL).

Sterile Discs of diameter 6 mm is placed on the surface of the middle of the Petri dish impregnated with each nanoparticle formulation (SC, SC3, and SC6) were carefully placed on the inoculated agar surfaceunder aspetic conditions. The plates were pre-incubated at 4 °C for 2 h to allow proper diffusion of the samples, then incubated at 37 °C for 24 h for bacterial strains and at 30 °C for 48 h for the fungal strain.

After incubation, the diameters of the inhibition zones (mm) were measured using a digital caliper. Each experiment was performed in triplicate (n = 3), and the mean ± standard deviation (SD) was calculated for each sample.

Controls

To ensure the reliability of the results, appropriate control conditions were included:

- Positive control: commercial antibiotic discs – Gentamicin (10 µg/disc) for bacteria and Amphotericin B (10 µg/disc) for fungi.
- Negative control: sterile discs impregnated with distilled water or the blank matrix without nanoparticles.
- The presence of a clear inhibition zone around the test or control discs indicated antimicrobial activity, while the absence of such a zone indicated microbial resistance.
- Minimum Inhibitory Concentration (MIC) Determination.

MIC is defined as the lowest concentration that can inhibit any microbial visible growth, the MIC was measured. A 96-well plate was divided into aliquots containing 100 µl of MH liquid medium. The MH liquid micro dilution method using 96-well ELISA plates was used.[31]

The procedure was performed according to the standard protocol,[32] with slight modifications. The minimum inhibitory concentration (MIC) is defined as the lowest concentration of nanoparticles or nanoparticle-based emulgel that causes a 90% reduction in microbial growth compared to the untreated control. These parameters were determined using the microdilution method in liquid Brain Heart Infusion (BHI) or Mueller-Hinton Broth (MHB) medium, to find the effects of the tested nanoparticles. A stock suspension of nanoparticles was prepared in DMSO or sterile distilled water at a final concentration of 100 mg/mL. A two-fold serial dilution was then performed from this stock to obtain a range of concentrations: 0.5, 0.25, 0.125, 0.0625, 0.0312, 0.0159, 0.0078, 0.0039, and 0.0019 mg/mL. From each dilution, 100 µL were distributed into the wells of a 96-well microplate, each well containing

100 µL of MHB. Subsequently, 20 µL of standardized bacterial inoculum (≈10^6 CFU/mL) were added to each well. Each row was reserved for a specific bacterial strain.

Two types of controls were included:

- Negative control: wells containing only 100 µL of sterile MHB (to check sterility).
- Positive control: wells containing 100 µL of MHB and 20 µL of bacterial inoculums without nanoparticles (to confirm bacterial growth).

After incubation at 37 °C for 24 hours, the MIC was determined as the lowest nanoparticle concentration showing no visible bacterial growth (turbidity), on agar plates.

Statistical Analysis

Data on inhibition zone diameters were analyzed using one-way ANOVA to compare the antimicrobial effects of the nanoparticle formulations containing 0%, 3%, and 6% Sr (SC, SC3, SC6) with the antibiotic discs (ATB). Statistical significance was set at $p < 0.05$, and analyses were performed using SPSS software.

RESULTS AND DISCUSSION

Characterization of synthesized materials

Figure 2 shows the X-ray diffraction patterns of undoped and Sr-doped Co_3O_4 powders heat-treated at 600°C for 4 hours. For all three samples, the peak positions are in good agreement with the reflections of the standard structure of cubic spinel Co_3O_4 (space group F-43m, JCPDS card N0. 42-1467).[33] The peaks observed at 2θ angles of 19.14°, 31.46°, 37.02°, 38.74°, 44.95°, 55.81°, 59.50° and 65.43° can be indexed for diffractions from the (111), (220), (311), (222), (400), (422), (511), and (440) planes.[34] No extradiffraction peaks were detected, indicating that no crystalline parasitic phases are present in the samples. In addition, slight shifts of the SC3 and SC6 peaks to lower 2θ values were observed compared to that of the undoped Co_3O_4 samples, indicating the replacement of Co^{2+} by Sr^{2+} into the Co_3O_4 crystal structures.[35]

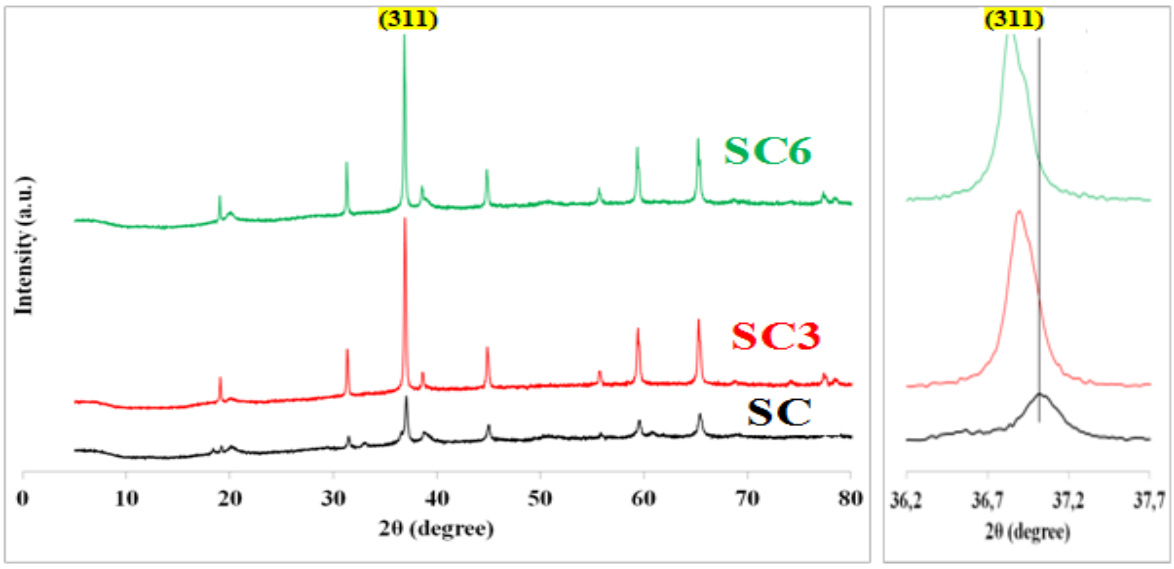

Fig. 2 – XRD patterns of pure and Sr-doped Co_3O_4 nanoparticles.

Based on line broadening analysis, the average crystallite size (D), lattice parameter (a), unit cell volume (V), dislocation density (δ) and micro-strain (ε) are calculated using Eqs. (1), (2), (3), (4) and (5) respectively:[36–40]

$$D = \frac{k\lambda}{\beta cos\theta} \quad (1)$$

$$a = d_{hkl}(h^2 + k^2 + l^2)^{1/2} \quad (2)$$

$$V = a^3 \quad (3)$$

$$\delta = \frac{1}{D^2} \quad (4)$$

$$\varepsilon = \frac{\beta}{4tan\theta} \quad (5)$$

The obtained values of the lattice parameter, unit cell volume, crystallite size, microstrain and dislocation density are presented in Table 1. The results indicate that the average particle size of Co_3O_4 increases with the increase in lattice volume caused by the increase in the amount of strontium incorporated on the one hand and the agglomeration

process on the other hand. While the dislocation density which remains inversely proportional to the average particle size decreases with increasing doping rate. We also observe that the microstrain of the doped samples is smaller than that of the undoped sample, showing a reduction for higher doping rates.

Table 1

Calculated value of lattice parameter and volume, average crystallite size, microstrain and dislocation density

	D (nm)	a (Å)	V (Å^3)	δx10^{14} (line/m^2)	ε x10^2 (rad)
Undoped	36,58	8,0474	521,1548	7,47	2,986
Sr (3%)	37,07	8,0736	526,2616	7,28	2,848
Sr (6%)	37,47	8,0745	526,4376	7,12	2,928

To study the effect of Strontium doping on vibrational properties of cobaltite oxide, FTIR spectroscopy experiments were carried out Shimadzu 8400 Spectrometer. The FTIR spectrum of pure and strontium doped Co_3O_4 nanocrystals synthesized through the sol-gel method was recorded in the range of 400–4000 cm^{-1}. As displayed in Fig. 3, the strong absorption peak at approximately 578 cm^{-1} corresponded to B-O vibrations, "B" represents Co^{3+} ions octahedral coordinated and the second one at 667 cm^{-1} corresponded to A-O type, "A" represented the metal Co^{2+} ions tetrahedral coordinated confirming the formation of spinel Co_3O_4 in pure phase.[41,42] The peak at around 1126 cm^{-1} is associated to O–H.[43] The band at 1634 cm^{-1} is ascribed to the structural deformation of absorbed water molecules[44] and the weak band at around 3413 cm^{-1} shows the stretching vibration mode of the O-H groups of H_2O from humidity.[45–47] Finally, the infrared spectrum of all samples shows no residual organic or inorganic compounds like strontium oxide.

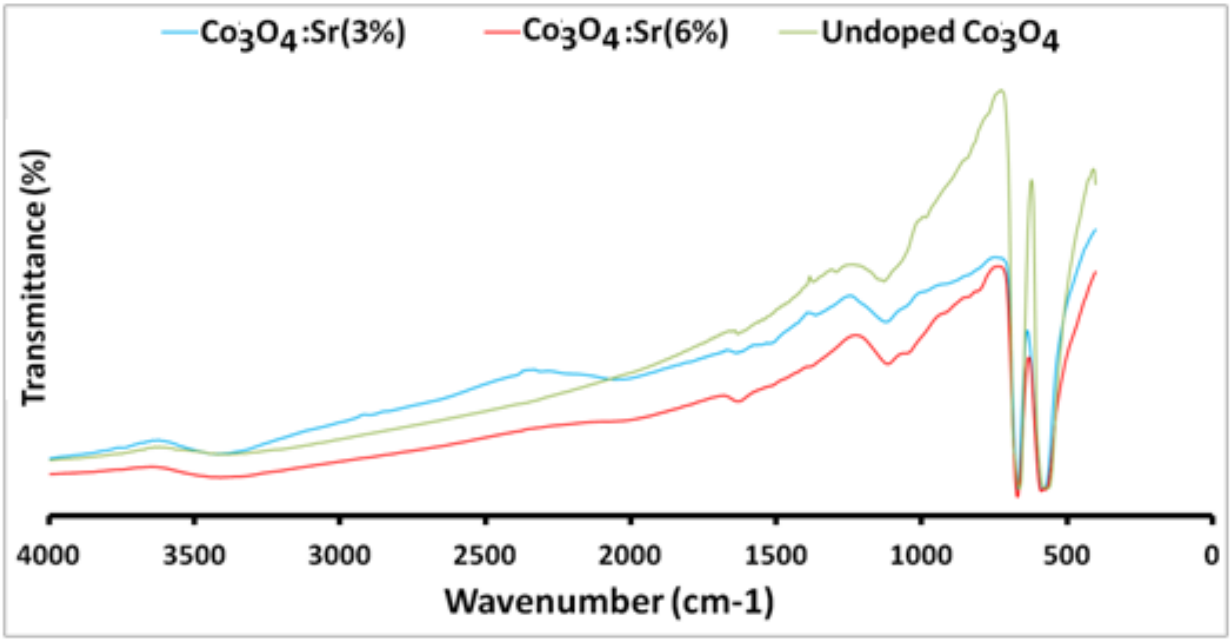

Fig. 3 – FTIR spectra of undoped and Sr-doped Co_3O_4.

In order to determine the shape of the developed nanoparticles, micrographs obtained by scanning electron microscopy are presented in Fig. 4. The particles are generally spherical in shape with more or less different sizes. This heterogeneous size dispersion is due to the formation of agglomerates caused by the charge state of the surfaces.

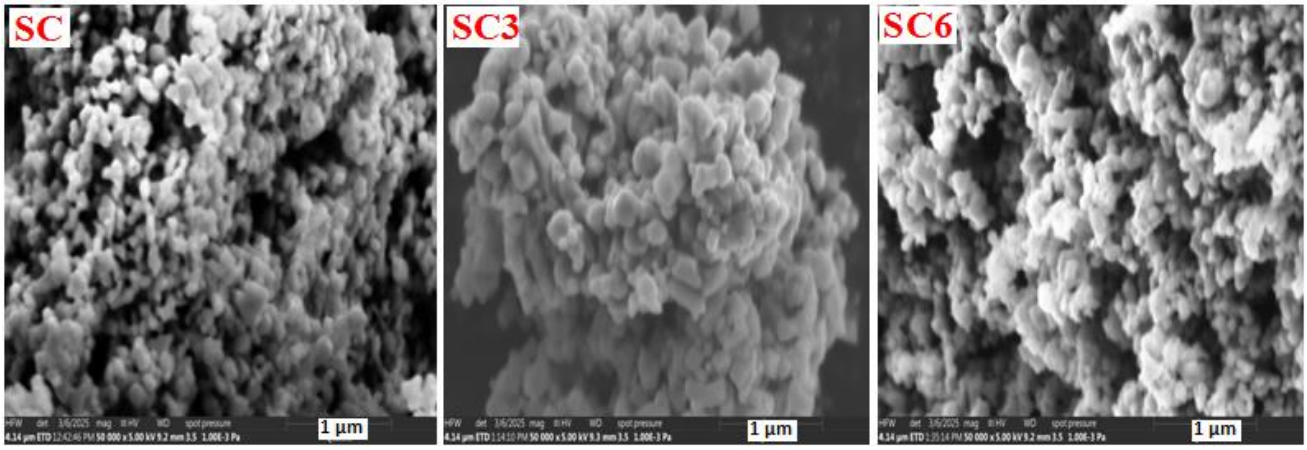

Fig. 4 – SEM Micrographs of undoped and Sr-doped Co_3O_4.

Antibacterial and antifungal activity

The antimicrobial performance of pristine Co_3O_4 (SC) and Sr-doped Co_3O_4 samples (SC3 and SC6) (Figs. 5, 6) showed a pronounced dependence on the Sr content. As summarized in Table 1, the inhibition zones systematically (Fig. 7) increased with Sr doping, indicating that the incorporation of Sr^{2+} ions significantly enchances the biological activity of the spinel oxide. The 6% Sr-doped material (SC6) exhibited the highest inhibition diameters against all tested strains, exceeding those of conventional antibiotics such as amoxicillin, ciprofloxacin, and ketoconazole.[48]

This improvement can be attributed to several physicochemical modifications induced by Sr incorporation in the Co_3O_4 lattice. The substitution of Co^{2+} by Sr^{2+} (larger ionic radius) causes lattice distortion and the generation of oxygen vacancies, which increase the surface defect density and active sites. These defects enhance the adsorption and interaction of the material with microbial cell walls, facilitating redox reactions and the production of reactive oxygen species (ROS) such as superoxide ($O_2^{-}\cdot$) and hydroxyl radicals ($\cdot OH$). The ROS induce oxidative stress, leading to membrane disruption, leakage of intracellular contents, and DNA damage in microbial cells. Furthermore, Sr doping alters the electronic band structure of Co_3O_4, improving charge separation and electron mobility at the surface, which enhances redox-driven antimicrobial processes. The partial release of Sr^{2+} and Co^{2+} ions into the surrounding medium may also contribute to the ionic toxicity effect, disturbing membrane potential and enzymatic activities of the microorganisms. The combined effects of increased oxygen vacancy concentration, enhanced ROS generation, and ion release account for the superior antimicrobial behavior of Sr-doped Co_3O_4, particularly at 6% Sr. Therefore, Sr substitution can be considered an effective strategy to tune the structural, electronic, and biological properties of cobalt oxide spinels for antimicrobial applications.

Table 2

Comparative analysis of the inhibition diameter of the Antibacterial and Antifungal Activity of Nanoparticles and Reference Antibiotics[2]

Strains	SC (mm)	SC3 (mm)	SC6 (mm)	Mean ± SD (mm)	Comparable Antibiotic (10 µL)	Typical Inhibition Zone (mm)
Candida albicans	23	25	29	25.7 ± 3.1	Ketoconazole	25
Staphylococcus aureus	15	17	28	20.0 ± 7.0	Amoxicillin	20
Escherichia coli	18	19	22	19.7 ± 2.1	Ciprofloxacin	20
Pseudomonas aeruginosa	17	18	26	20.3 ± 4.9	Amikacin	22

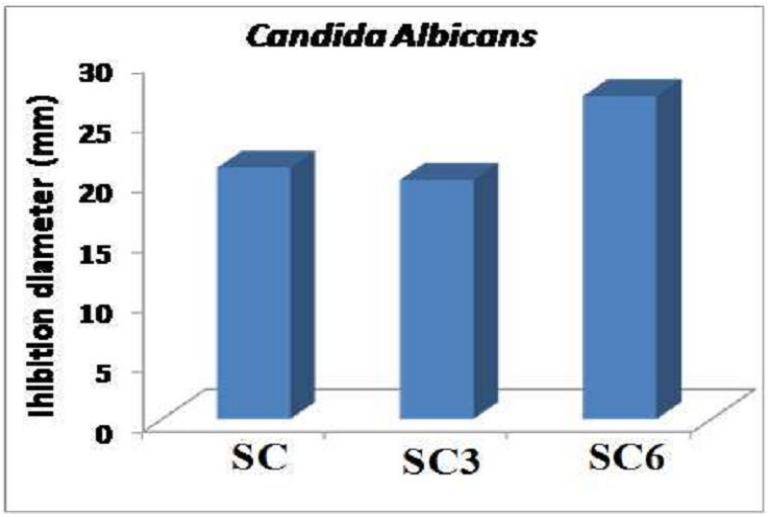

Fig. 5 – Antifungal activity of NPs.

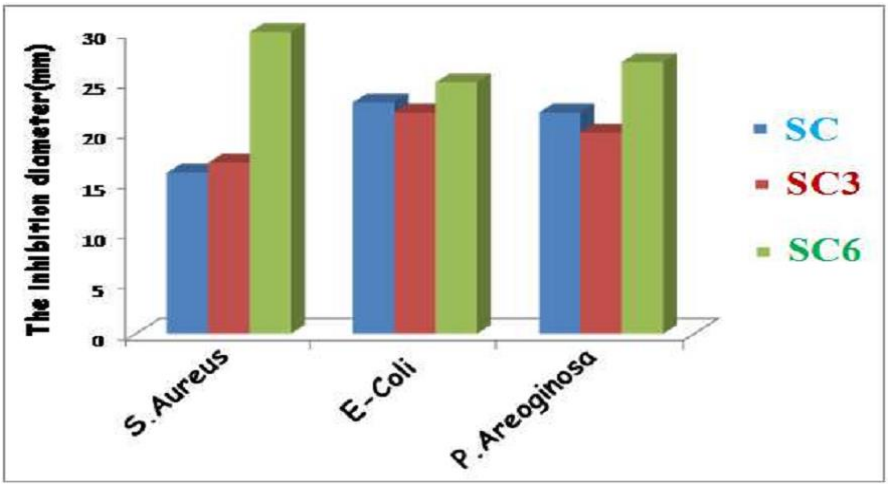

Fig. 6 – Antibacterial activity of NPs.

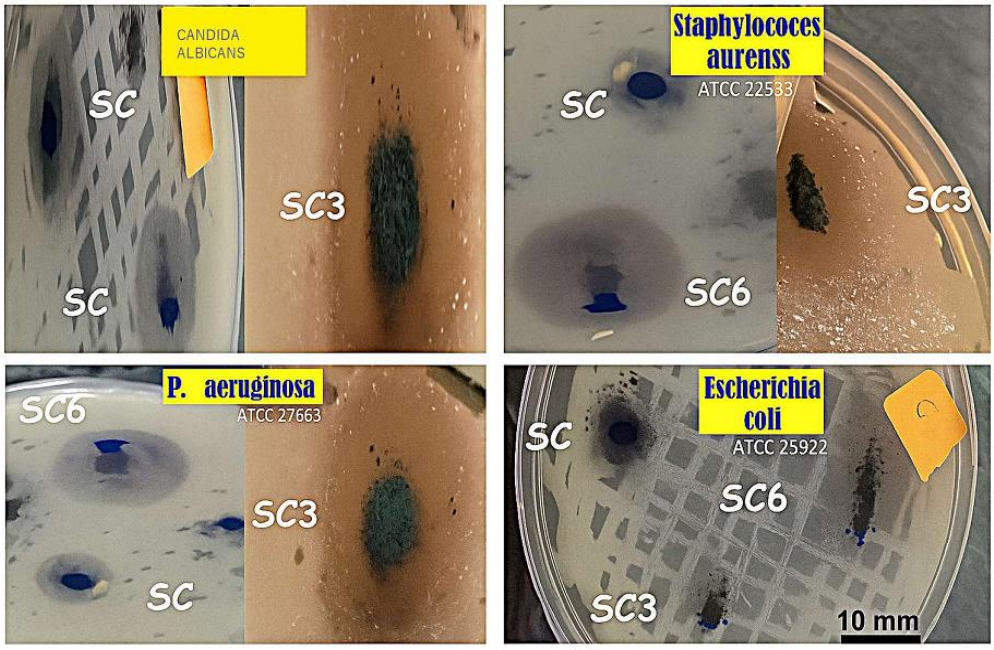

Fig. 7 – Antibacterial and antifungal activity of the SC, SC3, and SC6 formulations against *C. albicans*, *S. aureus*, *P. aeruginosa*, and *E. coli*. Magnification: ×100; Scale bar = 1 cm.

Minimum Inhibitory Concentration (MIC) Determination

The MIC evaluation shows that it remains relatively low (Table 2). It is between 3.12 and 6.25.mg/l. This concentration represents the concentration for which 90% of the bacterial population is eliminated. All three nanoparticles, are good products that can inhibit gram-positive and negative strains as well as the fungus. These results clearly show that the doping of cobalt oxide with strontium has a considerable effect on the MIC value of NPs. Interestingly, the SC6 sample exhibited the highest MIC value but also the largest inhibition zone diameter. This apparent discrepancy can be attributed to the physicochemical properties of Sr-doped Co_3O_4 nanoparticles. The increased strontium content in SC6 may enhance the surface charge and reactive oxygen species (ROS) generation, promoting rapid bactericidal activity on the agar surface, which results in a larger inhibition zone. However, in the liquid medium used for MIC determination, particle aggregation or limited dispersion may reduce their effective concentration in contact with microbial cells, leading to a higher MIC value. Therefore, the inhibition zone mainly reflects the surface diffusion and immediate contact activity, whereas the MIC expresses the minimum concentration required to completely inhibit microbial growth in a homogeneous environment.

Table 3

Minimum Inhibitory Concentration (MIC) of Co_3O_4 and Sr-Co_3O_4 NPs against antimicrobial strains

Strains Nps	CMI *S. Aureus* (G+)	CMI *E. Coli* (G-)	CMI *P. Aeruginosa* (G-)	CMI *C. Albicans* (G-)
SC	3.125	6.250	6.250	6.250
SC3	3.125	3.125	3.125	6.250
SC6	6.250	6.250	6.250	6.250

Comparison of the interaction of nanparticles with strains studied by zeta potential

The nanoparticles were characterized by a Zetasizer model (Malvern Instruments) to evaluate the zeta potential (Figs. 8 and 9), in order to find a correlation between the charge of the NPs and the variation of the inhibition diameters. It is observed that the zeta potential is negative for all the materials, with a lower value recorded for the SC6 sample.

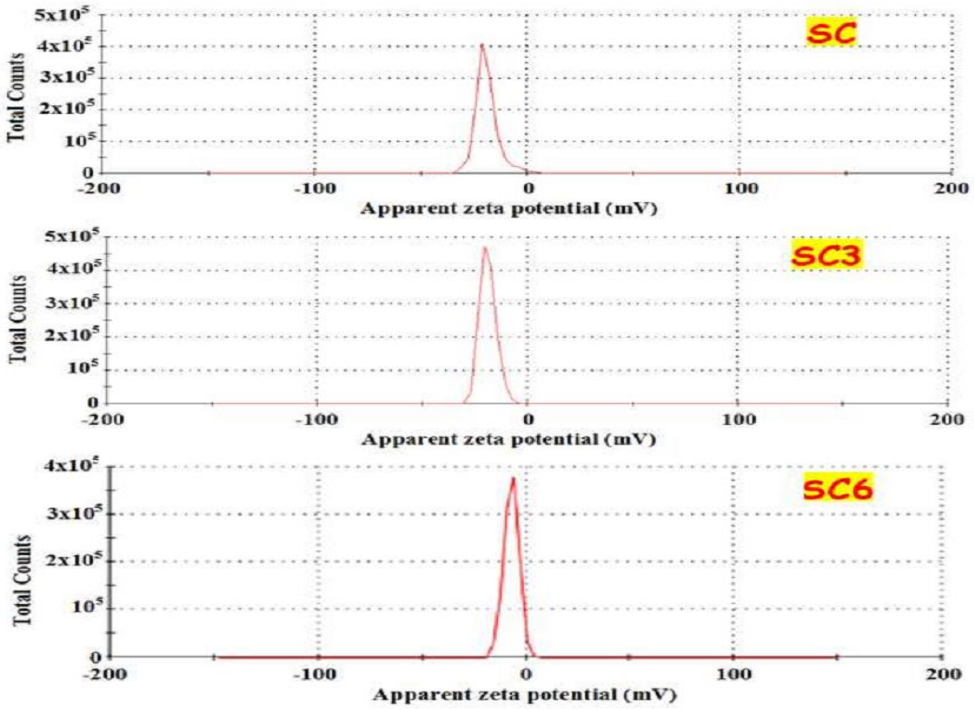

Fig. 8 – Total count *versus* apparent zeta potential (mV) for nanopaticles.

The electrostatic forces are responsible for the attraction between the bacteria and the fungus studied on one side and the charged surface of the nanoparticles of the materials (SC, SC3 and SC6) on the other side. Consequently, the resulting electrostatic adhesion leads to the direct death of these bacteria by rupture of the cytoplasmic membrane. This can be justified by the high values of the inhibition diameter (Table 1) recorded by the three powders, especially for the 6% doped sample. This result can be explained by the fact that strontium doping favors the appearance of charges by its greater electronegativity compared to that of cobalt.

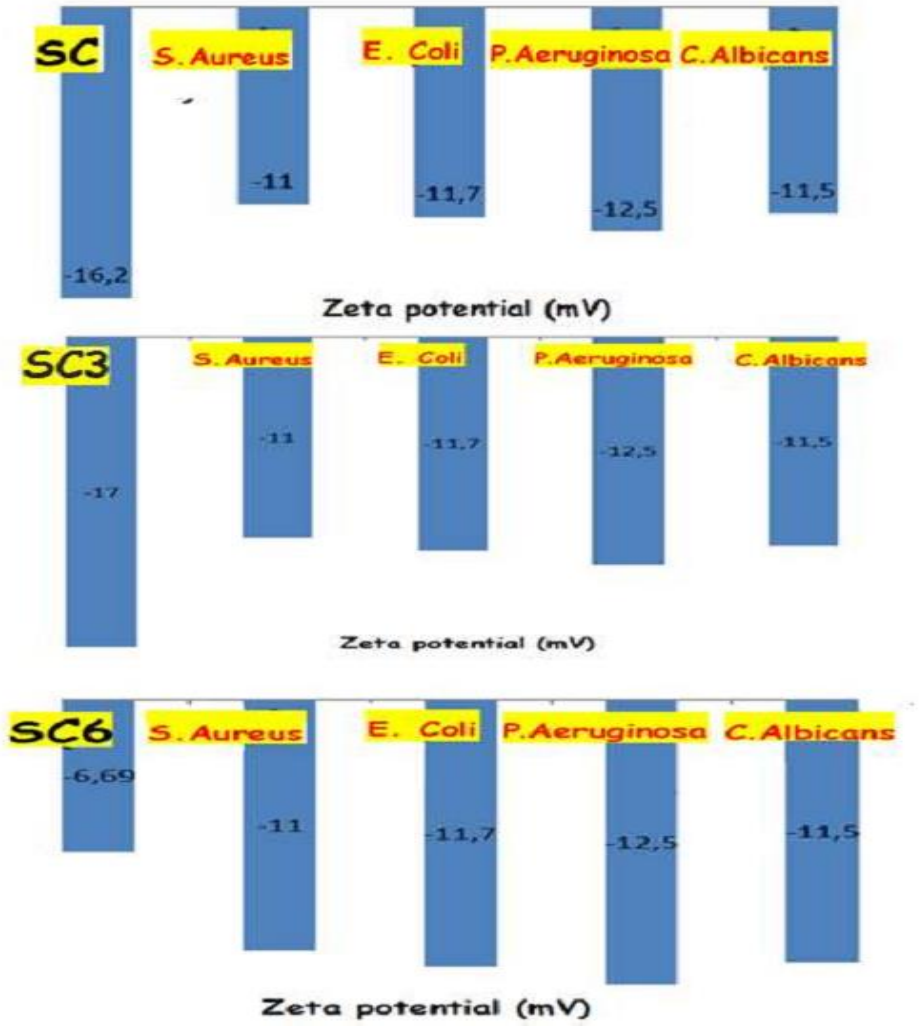

Fig. 9 – Zeta potential and inhibition diameter comparison for pure and Sr-doped Co_3O_4.

Zeta potential measurements revealed values of −16.2 mV for SC, −17.0 mV for SC3, and −6.69 mV for SC6 (Fig. 9), indicating that Sr doping significantly reduced the surface charge of the nanoparticles. The higher absolute values observed for SC and SC3 suggest better colloidal stability and electrostatic repulsion, whereas the near-neutral potential of SC6 promotes aggregation in suspension. This reduced electrostatic stability in SC6 can explain its higher MIC values (Table 2), as nanoparticle agglomeration in liquid medium limits the effective surface area available for microbial interaction. However, the same formulation exhibited the largest inhibition zones on agar plates, which may be related to localize release of Sr^{2+} ions and enhanced production of reactive oxygen species (ROS) at the nanoparticle cell interface. Therefore, while SC6 aggregates more in broth (raising MIC), its strong surface reactivity and ionic diffusion on solid medium lead to a larger inhibition halo. These findings confirm that zeta potential plays a critical role in balancing dispersion stability and antimicrobial efficiency of Sr–Co_3O_4 nanoparticles.

Statistical Analysis and Interpretation

The antimicrobial activity of the nanoparticle formulations containing different Sr concentrations (SC: 0%, SC3: 3%, and SC6: 6%) was statistically compared with that of the standard antibiotic discs (ATB). One-way ANOVA showed (Table 3) significant differences ($p < 0.05$) (Table 3) between treatments. The inhibition zones increased proportionally with the Sr content, reaching the highest values for SC6. In particular, SC6 (6% Sr) exhibited significantly greater activity (Figs. 5 and 6) than ATB against *Pseudomonas aeruginosa* ($p = 0.002$), *Candida albicans* ($p = 0.000$), *Staphylococcus aureus* ($p = 0.006$), and *Escherichia coli* ($p = 0.000$). These results confirm that increasing Sr concentration enhances the antimicrobial efficacy of the nanoparticles.

Table 4

Statistical comparison of inhibition zone diameters (mm) between nanoparticle formulations and antibiotic discs

Microorganism	SC	SC3	SC6	ATB (Antibiotic DISC)	SIG. (Bilateral)
Pseudomonas aeruginosa	17 ± 0.8	22 ± 0.6	26 ± 0.5	25 ± 0.7	0.002*
Candida albicans	21 ± 0.5	25 ± 0.4	29 ± 0.6	27 ± 0.5	0.000***
Staphylococcus aureus	19 ± 0.7	23 ± 0.5	28 ± 0.8	20 ± 0.6	0.006**
Escherichia coli	18 ± 0.6	20 ± 0.7	22 ± 0.5	20 ± 0.6	0.000***

Values are expressed as mean ± SD (n = 3). Statistical significance determined by one-way ANOVA followed by post-hoc test. (*$p < 0.05$; **$p < 0.01$; ***$p < 0.001$).

CONCLUSION

Pure and strontium-doped Co_3O_4 nanoparticles at 3 and 6% were prepared by sol-gel process and characterized by X-ray diffraction (XRD), Infrared spectroscopy (IR), Scanning electronic spectroscopy (SEM) and zeta-potential analysis. X-ray diffraction and infrared spectroscopy characterizations confirmed the formation of well-crystallized materials with a face-centered cubic spinel structure. The 3 and 6% strontium-doped Co_3O_4 retained the cubic spinel structure, which was identical to that of pure Co_3O_4. However, the size and morphology were inevitably influenced due to the ionic size and different electronic state of foreign atoms compared with those of the host cobalt in Co_3O_4. The Sr-doped Co_3O_4 nanoparticles exhibited remarkable antimicrobial efficiency against both Gram-positive and Gram-negative strains as well as *Candida albicans*. The 6% Sr-doped sample (SC6) showed the highest inhibition zones (29 mm) for *C. albicans*, (28 mm) for *S. aureus*, (26 mm) for *P. aeruginosa*, and (22 mm) for *E. coli*, surpassing the reference antibiotics ($p < 0.01$). The minimum inhibitory concentrations (MICs) ranged between 3.12 and 6.25 mg/L, confirming potent bactericidal and fungicidal activity at low doses. Zeta potential values decreased from −16.2 mV (SC) to −6.69 mV (SC6), indicating that Sr incorporation reduced surface charge and enhanced reactive oxygen species (ROS) generation. Statistical analysis (ANOVA, $p < 0.05$) confirmed that increasing Sr content significantly improved the antimicrobial performance of Co_3O_4 nanoparticles through synergistic effects of ionic release, surface reactivity, and oxidative stress induction.

Acknowledgements. We thank the Ministry of Higher Education and Scientific Research for the financial assistance allocated to research in Algeria. S. D. LAMBERT thanks the “Fonds National de la Recherche Scientifique” for her position as Research Director. The authors thank also the “Région wallonne” for its financial contribution.

REFERENCES

1. S. Khana, S. Ali, S. Muhammad, B. Khan, A. Ali, A E. Hesham and S. Begum., *Desalin. Water. Treat*., **2020**, *181*, 221.
2. S. Fahimirad, Z. Fahimirad and M. Sillanpää., *Sci. Total. Environ*., **2021**, *751*, 141673.
3. Y. Dutt, R. P. Pandey, M. Dutt, A. Gupta, A. Vibhuti, J. Vidic, V. S. Raj, C. M. Chang and A. Priyadarshin., *J. Nanobiotechnology*, **2023**, *21*, 148.
4. S. Kaushal, N. Thakur and K. Kumar, *J. Environ. Chem. Eng.*, **2025**, *13*, 116241.
5. P. Nagarajan and V. Rajagopalan., *J. Sci. Technol. Adv. Mater*., **2008**, *9*, 035004.
6. O. Toshiaki, Y. Osamu, I. Yasuhiro and N. Zenbe-e., *J. Mater. Sci. Mater. Med.*, **2008**, *19*, 1407.
7. Z. A. Zakaria, A. Mat Desa, K. Ramasamy, N. Ahmat, A. S. Mohamad, D. A. Israf and M. R. Sulaiman, *Afr. J. Microbial. Res.*, **2010**, *4*, 071–075.
8. A. Imtiyaz, A. Singh and R. Gaur, *Bio. Nano. Sci.*, **2024**, *14*, 3536.
9. L. J. Cardenas-Flechas, A. M. Raba and M. Rincón-Joya, *Rev. DYNA*, **2020**, *87*, 184.
10. T. R. Paudel, A. Zakutayev, S. Lany, M. d'Avezac and A. Zunger, *Adv. Funct. Mater*., **2011**, *21*, 4493.

11. I. Derkaoui, M. Achehboune, I. Boukhoubza, E. El Allam, Z. El Adnani, L. Henrard and A. Rezzouk, *Physica B: Condensed Matter*., **2023**, *660*, 414903.
12. R. Karthick, P. Sakthivel, C. Selvaraju and P. Mosae Selvakumar, *J. Nanomater*., **2021**, *2021*, 7 pages.
13. E. Munirathinam and Y. Thomas Chung-Kuang, *Int. J. Electrochem. Sci.*, **2019**, *14*, 2914–2924.
14. R. Jeba, S. Radhika, C. M. Padma and X. Ascar Davix, *Mater. Today : Proc.*, **2022**, *58*, 927–931.
15. I. Muhammad, S. Anum, B. Muhammad, H. Ali, Ul-H. Anwar, N. Walid, H. Junaid, A. Salamat, M. Francisco and I. Muhammad, *Front. Chem.*, **2023**, *11*, 167701.
16. Ki. Farwa Ahmad, S. Umair, B. Amin, T. Saira, A. Misbah and P. Jahangir Ali, *Artif. Cells. Nanomed. Biotechnol*., **2018**, *46*, S1083–S1091.
17. S. P. Keerthana, R. Yuvakkumar, G. Ravi, M. Thambidurai, D. N. Hung and V. Dhayalan, *RSC Adv*., **2023**, *13*, 18779–18787.
18. A. Ateeq, M. Naseem Siddique, A. Umair, T. Ali and P. Tripathi, *Appl. Surf. Sci.*, **2019**, *463*, 976–985.
19. S. R. Ali, R. Kumar and A. Kalam, *Arab. J. Sci. Eng.*, **2019**, *44*, 6295.
20. S. Mammeria, O. Halimia, M. Sebais, S. Touahri, B. Boudine, A. Azizic and M. T. Soltani, *Phys. Chem. Res.*, **2023**, *11*, 559.
21. J. O. Sunday, O. Magdalena, M. K. Agnieszka, N. Dorota, K. Michal, P. Marek and K. Pawel, *Ceram. Int.*, **2023**, *49*, 19851.
22. R. Radheshyam, C. Indrani, M. A. Valente and L. K. Andrei, *Adv. Mater. Lett.*, **2013**, *4*, 354.
23. P. Anindya Sundar, K. Natarajan Vinoth, B. Dipankar, D. Mahuya and Q. Mohammad, *Mat. Letters.*, **2014**, *131*, 125.
24. I. A. Abdel-Latif, L. A. Al-Hajji, M. Faisal and A. Ismail, *Sci. Rep*., **2019**, *9*, 13932.
25. S. Kanithan, N. A. Vignesh, S. Baskar, S. Nagaraja, M. Abbas, A. Aabid and M. Baig, *Materials.*, **2022**, *15*, 8180.
26. M. Henni, S. Kadi and H. Benhabal, *Surf. Rev. Lett.*, **2022**, *29*, 2250048.
27. P. Debapriya, P. Prafulla Kumar, M. Aishwarya, F. Ermelinda and D. Suresh Kumar, *Environ. Qual. Manag.*, **2022**, *2022*, 1.
28. K. Petcharoen and A. Sirivat, *Mater. Sci. Eng. B.*, **2012**, *177*, 421.
29. H. Abbas, K. Nadeem, A. Hafeez, A. Hassan, N. Saeed and H. Krenn., *Ceram. Int.* **2019**, *45*, 17289.
30. D. A. Ward and E. I. Ko, *Ind. Eng. Chem. Res.* **1995**, *34*, 421.
31. H. Mustafa, S. Rulla and H. H. Esam, *Int. J. Drug Deliv. Technol*., **2023**, *13*, 995.
32. L. Bennabi, F. Debab, F. Bennabi, I. Abdelmalek, K. Guemra, L. Belarbi, A. Dehbi, A. Alsalme and M. Messori., *Appl. Biochem. Biotechnol.* **2025**, *197*, 4969.
33. G. Lanlan, C. Fang, X. Ning, W. Chong, K. Xueying, S. Yanfeng, M. Jian, L. Xishuang, G. Yuan and L. Geyu, *J. Colloid Interface Sci.*, **2018**, *528*, 53–62.
34. G. Hitkari, S. Sandhya, P. Gajanan, K S. Manoj and K. Deepak, *J. Mater. Sci. Eng*., **2018**, *7*, 1000419.
35. O. Bilgili, *Acta Phys. Pol. A*., **2019**, *136*, 460.
36. N. Guermat, W. Daranfed, I. Bouchama and N. Bouarissa, *J. Mol. Struct*., **2021**, *1225*, 129134.
37. W. Darenfad, N. Guermat and K. Mirouh, *J. Mol. Struct.*, **2023**, *1286*, 135574.
38. M. S. Othman, K. A. Mishjil, H. G. Rashid, S. S. Chiad, N. F. Habubi and I. A. Al–Baidhany, *J. Mater. Sci.: Mater. Electron*., **2020**, *31*, 9037–9043
39. W. Darenfad, N. Guermat and K. Mirouh, *J. Nano-Electron. Phys.*, **2021**, *13*, 06016.
40. M. Khalfallah, N. Guermat, W. Daranfed, N. Bouarissa and H. Bakhti, *Phys. Scr*., **2020**, 95, 095805.
41. S. N. Karthick, K. V. Hemalatha, C. Justin Raj, H. J. Kim and M. Yi, *J. Nanopart. Res.*, **2013**, *15*, 1474.
42. N. Bharati, K. Subhash, S. Mahesh and N. Arti, *J. Compos. Mater.*, **2013**, *47*, 559–567.
43. W. Ababay Ketema, A. Delele Worku, H. Nigus Gabbiye and Y. Temesgen Atnafu, *Heliyon*., **2021**, *7*, e08076.
44. S. Savitha, S. Surendhiran, K. S. G. Jagan, A. Karthik, B. Kalpana and R. Senthilmurugan, *J. Mater. Sci.: Mater. Electron.*, **2023**, *34*, 89.
45. R. M. Obodo, E. O. Onah, H. E. Nsude, A. Agbogu, A. C. Nwanya, I. Ahmad, T. Zhao, P. M. Ejikeme, M. Maaza and F. I. Ezema, *Electroanalysis.*, **2020**, *32*, 2786–2794.
46. N. Padmanathan, S. Selladurai and K. M. Razeeb, *RSC Adv*., **2015**, *5*, 12700–12709.
47. W. Jia, J. Li, Z. Lu, Y. Juan and Y. Jiang, *Materials*., **2018**, *11*, 1–20.
48. Clinical and Laboratory Standards Institute (CLSI). Performance Standards for Antimicrobial Susceptibility Testing, 33rd Edition, CLSI Supplement M100, 2023.